TR(BR)-2/97-98

Soil Erosion and Sediment Yield Modelling Using Kinematic Wave in GIS Environment

आपो हि ष्ठा मयोभुवः

NATIONAL INSTITUTE OF HYDROLOGY
JAL VIGYAN BHAWAN
ROORKEE - 247 667 (U.P.) INDIA

1997-98

CONTENTS

List of Figures

List of Tables

ABSTRACT

GIS techniques have been utilized to spatial discretization of a catchment in to time-area segments to be used in numerical solutions of the governing differential equations for rainfall-runoff-erosion process. Various thematic layers such as soil, landuse, slope, flow direction, DEM were generated for the Karso catchment using various tools available in GIS. These thematic layers were further utilized to generate attribute information such as Manning's n, USLE K and C parameters for use in rainfall-runoff-soil erosion model. Based on DEM and related attributed information of the catchment, time-area map of the catchment was prepared and used for spatial discretization of the catchment.

Rainfall abstraction has been carried out by phi-index method. The excess rainfall falling on each of the time-area segments was routed to outlet using numerical solutions of kinematic wave equation using fully implicit four-point finite difference scheme. The sediment yield has been estimated by solving sediment continuity equation using fully implicit finite difference scheme. Comparison of results indicated applicability of this modelling concept for Karso catchment.

1. INTRODUCTION

Soil erosion is among the most critical environmental hazards of modern times. Vast areas of land now being cultivated, may be rendered unproductive or atleast economically unproductive, if erosion continues unabated. Information on the sediment yield at the outlet of a river basin can provide a useful perspective on the rate of soil erosion and soil loss in the watershed upstream. Soil erosion involves detachment, transport and subsequent deposition (Meyer and Wischmeier, 1969). Soil is detached both by raindrop impact and the shearing force of flowing water. Sediment is transported down slope primarily by flowing water, although there is a small amount of downslope transport by raindrop splash. Runoff and downslope transport does not occur until rainfall intensity exceeds infiltration rate. For this reason soil erosibility decreases as infiltration rate increases. Once runoff starts, the quantity and size of material transported increases with the velocity of runoff water. At some point downslope, slope may decrease, resulting in a decreased velocity and transport capacity. At this point, sediment will be deposited, starting with the large particles and aggregates. Smaller particles and aggregates will be carried further downslope, resulting in what is known as enrichment of fines.

Models available in the literature for sediment yield estimation can be grouped in to two categories (a) physically based models (b) lumped models. Generally in physically based models the ground surface is separated into inter-rill and rill erosion areas. Detachment over inter-rill areas is considered to be by the impact of rain drop because flow depth are shallow, while runoff is considered to be the dominant factor in rill detachment and sediment transport over both rill and inter-rill areas. The physically based models include AGNPS (Young et al., 1987), ANSWERS (Beasley et al., 1980), WEPP (Nearing et al., 1989) and SHETRANS (Abott et al. 1986, Wicks and Bathrust, 1996). The physically based models are expected to provide reliable estimates for the sediment yield. However, these models require the coordinated use of various sub-models related to meteorology, hydrology, hydraulics and soil. As a result, the number of input parameters for some of

these models is high. Therefore, practical application of these models are still limited because of such uncertainty in model parameters and also due to difference between the scale of application i.e. a catchment and that of the development i.e. a field (Hadley et al., 1985; Wu et al., 1993).

Alternatively, the lumped models such as Universal Soil Loss Equation (USLE) (Wischmeier and Smith, 1978), Modified Universal Soil Loss Equation (MUSLE) (Williams, 1978) or Revised Universal Soil Loss Equation (RUSLE) (Renard et al., 1993), combine the erosion from all processes over a catchment into one equation. Rainfall characteristics, soil properties, and ground surface conditions are represented by empirical constants in these methods. The lumped methods of sediment yield estimation are in frequent use in many parts of the world (Bogardi et al., 1986; Julien and Tango, 1994; Kothyari et al., 1996).

Geographic Information Systems (GIS) link land cover data to topographic data and to other information concerning processes and properties related to geographic location. When applied to hydrologic systems, nontopographic information can include description of soils, land use, ground cover, ground water conditions, as well as man-made systems and their characteristics on or below the land surface. A number of studies have been carried out in the past wherein the soil rates were determined using the USLE and the GIS (Bocco et al., 1988; Omakupt, 1989; Jurgens et al., 1993; Jain et al., 1995). In the present study, GIS techniques has been utilized for spatial discretization of a catchment into time area segments by computing time of travel from individual grid to reach out let of the watershed and reclassification of time travel map into isochrone map. The GIS techniques are also utilized for determination of those physical parameters of individual time area segment such as slope, length, width, USLE parameters etc. that are related to the soil erosion. Surface erosion is then computed within the individual time -area segment using expressions for sediment detachment and transport. Next, the eroded sediment is routed to the catchment outlet by sediment continuity equation.

2. MATHEMATICAL FORMULATION

The one-dimensional partial differential equations employed in the present study for rainfall-runoff-erosion modeling are given below:

2.1 Overland Flow

The processes of soil detachment and transport are strongly influenced by the flow dynamics. Consider that w is the width of an elementary strip in the catchment and h is the flow depth. Assuming uniform distribution flow over the width due to the effective rain, i_e, continuity equation for flow is given as below (Field, 1982).

$$\frac{\partial Q}{\partial x} + w\left[\frac{\partial h}{\partial t}\right] = w \times i_e \qquad \ldots 1$$

Here Q is the inflow in the direction x and t is time. If all the changes in momentum flux and pressure are neglected then the momentum equation reduces to (Henderson, 1966)

$$S_f = S \qquad \ldots 2$$

Here S_f is friction slope and S is the bed slope. Under these conditions flow cross-sectional area A can be expressed as a power function of discharge (Chow et al., 1988) as

$$A = \alpha Q^{\beta} \qquad \ldots 3$$

The coefficient α and β are called the kinematic wave parameters. According to Manning's equation, $\beta = 2/3$ and, in SI units:

$$\alpha = \frac{1}{n\xi^{2/3}} S^{1/2} \qquad \ldots 4$$

where n = Manning's roughness coefficient, ξ is proportion of catchment width comprising the wetted perimeter of channel flow (Field, 1982). Since in most of the catchment applications it is difficult to evaluate n and ξ separately, the effective roughness is defined (Field and Williams, 1983) as,

$$\eta = n \cdot \xi^{2/3} \qquad \ldots 5$$

so that eq. 4 becomes

$$\alpha = \frac{S^{1/2}}{\eta} \qquad \ldots 6$$

These relations can be combined to produce the kinematic wave equation for flow given as below:

$$\frac{\partial Q}{\partial x} + \alpha\beta Q^{\beta-1}\frac{\partial Q}{\partial t} = w \times i_e \qquad \ldots 7$$

In the present study x is the distance measured along the main channel (Fig. 1) from the most remote point on the catchment divide and w is the width of catchment at distance x, measured along the isochrone which represents the time of travel of kinematic wave to the catchment outlet. The time value of isochrone passing through given x may change through the course of a storm event. However, under the assumption of aerial uniformity of rainfall excess its shape will remain unchanged in which case $w = w(x)$ (Field, 1982).

2.1.1 Non-dimensional form

The order of magnitude of various terms appearing in Eq. 7 could be largely different in problems involving real data. However it is considered that the order of magnitude of various terms in non-dimensional form of the equation will not vary much from each

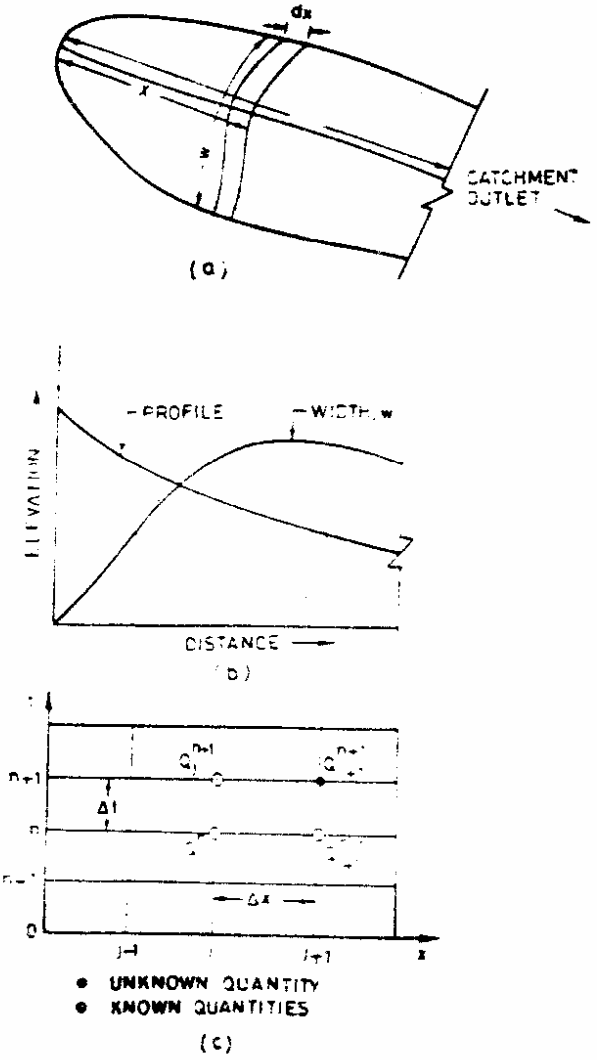

Fig. 1. Definition sketch. (a) Plan view of catchment; (b) main stream profile and area shape diagram and (c) x–t plane.

other. Hence it is appropriate to solve Eq. 7 in its non-dimensional form. As per Field (1982) the following steps have been taken for this purpose.

The length of main stream l is considered as the characteristic length, thus x can be non-dimensionalized by defining

$$x' = x/L \qquad \ldots 8$$

If P_e, which is the average intensity over the storm, is considered as the characteristic rainfall intensity, and A_r, is the catchment area then non-dimensional flow discharge is

$$Q' = \frac{Q}{A_r P_e} \qquad \ldots 9$$

Non-dimensional flow width

$$w = w/\overline{w} \qquad \ldots 10$$

where $\overline{w}$ is the average width of the catchment. Time t is non-dimensionalized by the time of concentration for the catchment T_c.

Let the catchment be divided into segments of length L_i, slope S and effective roughness η_i, then the velocity of flow,

$$V_i = \frac{L_i}{t_i} \qquad \ldots 11$$

Also V_i can be determined as per Manning's equation by taking the average value of flow depth h as equal to $P_e \cdot T_c$ Accordingly;

$$V_i = \frac{1}{\eta_i}(P_e \cdot T_c)^{2/3} S_i^{1/2} \qquad \ldots 12$$

Therefore,

$$\frac{L_i}{t_i} = \frac{P_e^{2/3} T_c^{2/3} S_i^{1/3}}{\eta_i} \qquad \ldots 13$$

as $\sum t_i = T_c$ it follows that

$$T_c = \eta_e^{0.6} P_e^{-0.4} (L/S_e^{1/2})^{0.6} \qquad \ldots 14$$

Here $L = \sum L_i$ and S is the equivalent uniform slope of the catchment and η_e, is the equivalent effective roughness for the catchment. These are given by the following equations:

$$S_e = \left\{ \frac{L}{\sum \left[\frac{L_i}{S_i^{1/2}} \right]} \right\}^2 \qquad \ldots 15$$

and

$$\eta_e = (S_e^{1/2}/L) \left[\sum \left(\frac{\eta_i L_i}{S_i^{1/2}} \right) \right] \qquad \ldots 16$$

and t is non-dimensionalized by defining $t' = t/T_c$ and has been non-dimensionalized as:

$$\alpha' = (\alpha \cdot L^{3/5}) / w^{2/5} P_e^{2/5} T_c \qquad \ldots 17$$

which according to Manning's equation reduces to:

$$\alpha' = \left[\frac{\eta_i}{\eta_e} \right]^{3/5} \left[\frac{S_e}{S_i} \right]^{3/10} \qquad \ldots 18$$

Excess rainfall intensity has been non-dimensionalized by average intensity of the rainstorm as

$$i' = i_e / P_e \qquad \ldots 19$$

Now Eq. 7 is written in the equivalent non-dimensionalized form as below:

$$\frac{\partial Q'}{\partial x'} + \alpha' \beta Q'^{\beta-1} \frac{\partial Q'}{\partial t'} = w' \cdot i_e' \qquad \ldots 20$$

The above equation is quite convenient for computational purpose. For getting the output again, the non-dimensional value can be multiplied by $A_t \cdot P_e$.

2.1.2 Numerical solution

Given the kinematic wave friction parameters α' and β the lateral inflow which is equal to $w' \cdot i_e'$. Eq. 20 is solved for $Q'(x', t')$ at each point on the $x' - t'$ grid to determine the hydrograph Q *(L,t)* at the outlet using the initial and boundary conditions.

2.1.3 Numerical grid used for computations

The temporal variation i.e. the storage delay of an input at the catchment outlet can be estimated by the catchment time area curve (Laurenson 1964). This method also accounts for the time intensity variation and aerial distribution of rainfall (Linsley et al, 1958). In order to utilized the potential of time area segment for computation of temporal variation of sediment yield the spatial grid for numerical computation is formed using the time area segments. For this, value of the time increment Δt is decided first. Isochrone are then drawn over the catchment such that time of concentration of surface runoff between two successive isochrones is Δt. Distance between these isochrones becomes the Δx value in the numerical grid. Thus the resulting grid will have changing value of Δx with the distance. In Fig. 1 the definition of a time area element is given on the top and the middle

portion depicts the variation in widths and lengths of the elementary time area profiles along the main stream while the bottom portion depicts the non-uniform grid which is formed by the time area segments and is used for numerical computations. Let $\Delta x_i'$ be the non-dimensional space increment on the $x'-t'$ grid as per Fig. 1 then by using a fully implicit four-point finite difference scheme. Eq 20 can be written as below (Chow et al 1988):

$$\frac{\Delta t'}{\Delta x_{i+1}'} Q_{i+1}'^{j+1} + \alpha_{i+1}' \left[Q_{i+1}'^{j+1}\right]^{\beta} = \frac{\Delta t'}{\Delta x_{i+1}'} Q_i'^{j+1} + \alpha_{i+1}' \left[Q_{i+1}'^{j}\right]^{\beta} + \Delta t' \left[\frac{ql_{i+1}'^{j+1} - ql_{i+1}'^{j}}{2}\right] \quad \ldots 21$$

Here ql' is the non-dimensional form of lateral flow, which is equal to $w' \cdot i_e'$. Eq. 21 is a non-linear equation in $Q_{i+1}'^{j+1}$. Newton's iterative procedure has been used for its solution for spatially varying roughness and temporally varying inflows. This solution is unconditionally stable and a wide range of $(\Delta t'/\Delta x')$ values can be used without introducing large errors in the shape of the computed hdrograph (Chow et al, 1988). The initial estimate for $Q_{i+1}'^{j+1}$ to be used in non-linear scheme (iterations) has been obtained by using a linear scheme for solution in which case $\beta = 1$.

2.1.4 Initial and boundary conditions

Initially i.e. at $t' = 0$ the flow is equal to zero at all the points in the space domain in a dry catchment therefore

$$Q'(x',0) = 0 \text{ for } 0 \le x' \le 1, \text{ at } t' = 0 \quad \ldots 22$$

For a wet catchment the value of initial flow or base flow should be known. In that case $Q'(x',0) = Q_x'$ Similarly the discharge is zero from the upper most point of the space

domain for all time t' because only small headwater catchments are studied in the present study. Thus:

$$Q'(0,t') = 0 \text{ for } t' > 0 \qquad \ldots 23$$

The output of the above mode produces the $Q'(x',t')$. Making use of the appropriate definitions given previously, dimensionalization of output is done. As uniform conditions are assumed to exist over the width of catchment, the discharge per unit width and average velocity for each time area segment can be computed which become input to the sediment model. Flow depths and flow velocities are then computed at the grid points using Meaning's relationship.

2.2 Soil Erosion and Sediment Routing

Soil erosion is a complex process consisting of detachment of soil particles and their transport down slope. Eroded sediment deposits enroute if the transport capacity of the flow is inadequate. Here the flow of sediment laden runoff is treated as one dimensional, unsteady phenomenon. Imbalances between sediment supply and transport capacity cause erosion or deposition in the catchment. These processes are interrelated and must satisfy locally the conservation principle of sediment mass expressed by sediment continuity equation. The continuity equation for sediment is solved while keeping track of soil erosion and deposition in the flow elements. Finally sediment discharge at the catchment outlet is determined.

2.2.1 Sediment continuity equation

The continuity equation normally used in dynamic erosion model is given below (Bennett, 1974; Foster, 1982).

$$\frac{\partial q_s}{\partial x} + \rho_s \frac{\partial (C_c h)}{\partial t} = D_I + D_F \qquad \ldots 24$$

Here q_s is the sediment load mass per unit width per unit time, x is the distance along the slope, ρ_s is the mass density of the sediment particles, C_c is the averaged concentration of the sediment in the flow, h is the flow depth, t is the time, D_F is the rill erosion rate (mass per unit area per unit time) and D_I is the delivery rate of sediment from interrill areas (mass per unit area per unit time). The term $\partial q_s/\partial x$ is the build up or loss of sediment load with distance and $\partial(C_C h)/\partial t$ is the storage rate of sediment within the flow depth and D_I and D_F are the contributions from lateral inflow. Since $q_s = \rho_s C_c q$ and $q = V \cdot h$ the above equation can be written as

$$\frac{\partial q_s}{\partial x} + \frac{\partial (q_s / V)}{\partial x} = D_I + D_F \qquad \ldots 25$$

Where q is the discharge per unit width and V is the flow velocity.

2.2.2 Numerical solution

No general analytical solution to above equation exists. For the actual conditions the solution is usually made numerically using finite difference scheme. For this, the catchment is divided into number of time area segments. Similar to runoff simulation, sediment processes are also simulated in each of these segments. The computation sequence is also kept the same as used for runoff component. The finite difference scheme is used for solution of Eq. 25, with a typical grid in time and space as adopted in case of rainfall-runoff model (See Fig. 1). The finite difference form of the Eq. 25 is as under (Foster, 1982).

$$\begin{aligned}
&\left[\frac{q_{si+1}^{j+1} - q_{si}^{j+1}}{\Delta x_{i+1}}(1-a) + \frac{q_{si+1}^{j} - q_{si}^{j}}{\Delta x_{i-1}}(a)\right] \\
&\quad + \left[\frac{A_{si+1}^{j+1} - A_{si}^{j+1}}{\Delta t}(1-b) + \frac{A_{si}^{j+1} - q_{si}^{j}}{\Delta t}(b)\right] \qquad \ldots 26 \\
&\quad = (1-b)D_{Ii+1}^{j+1} + (b)D_{Ii+1}^{j} + (1-b)D_{Ii+1}^{j} + (b)D_{Ii}^{j} + (1-b)D_{Fi+1}^{j+1} \\
&\quad\quad + (b)D_{Fi}^{j+1} + (1-b)D_{Fi+1}^{j} + (b)D_{Ii}^{j}
\end{aligned}$$

Here A_s is given by q_s/V; a is the space weighting factor, b is the time weighting factor, x and t are space increment at jth node and time increment respectively, q_{si}^{j} is the quantity q_s at grid point $x = j$; Δx_j and $t = n \cdot \Delta t$. When weighting factors a and b are both zero. Eq. 26 becomes a fully implicit scheme (as used for rainfall-runoff model) and then it has q_{si+1}^{j+1} as the only unknown. The other values are known from previous computations, initial and boundary conditions; else they are determined through the rainfall-runoff model.

2.2.3 Initial and boundary conditions

It is considered that initially flow is not carrying sediment, i.e.

$$q_s(x,0) = 0 \text{ for } 0 < x < L \qquad \ldots 27$$

and also,

$$q_s(0,t) = 0 \text{ for } t > 0 \qquad \ldots 28$$

It implies that similar to runoff the inflow of sediment to the catchment is zero at the uppermost point.

2.2.4 Detachment by raindrop impact

When raindrop strikes the soil surface, soil particles are dislodged by the impact of rainfall. The rate of detachment by raindrop is generally proportional to the square of rainfall intensity (Beasley et al, 1980). The detachment due to raindrop impact is considered

$$D_i = C_{f1} \cdot C \cdot K \cdot A_i \cdot I^2 \qquad \ldots 29$$

Here D_I is the rainfall impact detachment rate (kg min^{-1}), C is the cover and management factor, a parameter of the Universal Soil Loss Equation (USLE, Wichmeier and Smith, 1978), K is the soil erodibility factor (another parameter of the USLE), A is the area increment (m^2), I is the rainfall intensity (mm/min) and C_{f1} is a coefficient, the value of which is to be optimized during calibration of the model.

2.2.5 Detachment by flow

Detachment of soil particles by flow occurs when the shear stress at the ground surface overcomes the gravitational and cohesive forces of the soil particles. Generally this detachment rate is proportional to both the surface slope and flow rate (Beasley et al, 1980). The detachment by flow is considered to be given by

$$D_F = C_{f2} \cdot C \cdot K \cdot A_i \cdot S \cdot q \qquad \ldots 30$$

Here D_F is the flow detachment rate (kg/min), S is slope and q is the flow rate per unit width (m/min), and C_{f2} is another coefficient, value of which is determined by calibration.

2.2.6 Transport capacity of the flow

The sediment load at catchment outlet is controlled by the amount of sediment made available for transport by detachment process and by the transport capacity of the flow (Meyer and Wischmeier, 1969). Factors controlling sediment transport capacity can be grouped into three categories: fluid properties, sediment characteristics and hydraulic parameters associated with the flow path. Chang (1988) described how the motion of a particle is controlled by two opposing forces: the applied force and resisting force. Beasley et al (1980) compared the different relationships for transport capacity. They suggested equations for the transport capacity in terms of the discharge and the slope. Nevertheless to account for the effect of changing hydraulic parameters, in other words the resisting force, in the catchment, the transport capacity is also considered to be a function of the C parameter of the USLE. Therefore following empirical equations as per

Beasley et al. (1980) are assumed to hold good for the transport capacity of the flow T_R (Kg/min/m)

$$T_R = Ca_1 \cdot S \cdot C \cdot q^{1/2} \text{ for q } < 0.046 \text{ m}^2 \text{ min}^{-1} \quad \ldots 31$$

$$T_R = Ca_2 \cdot S \cdot C \cdot q^2 \text{ for q } > 0.046 \text{ m}^2 \text{ min}^{-1} \quad \ldots 32$$

Here Ca_1 and Ca_2 are coefficients, values of which are considered to be the same as given by Beasley et al. (1991). The sediment load going out of any time area segment is limited by transport capacity of the flow in that segment. Hence, if sediment availability exceed the transport capacity, then excess sediment is left behind by flow in the corresponding time area segment.

3. THE STUDY AREA AND DATA AVAILABILITY

For the present study, the Karso catchment in the Barakar basin has been selected due to availability of data. The stream named Kolhuwatari traverses through this catchment and finally joins the Barhi nadi, a tributary of Barakar river. The total area of the catchment is 27.93 sq. km.

3.1 Location

Geographically this catchment lies between longitudes 85°24'20" East and 85°28'6" East and latitudes 24°16'47" North and 24°12'18" North as shown in the Fig. 2. The catchment is near the Tilaiya reservoir, which is built on the river Barakar.

3.2 Climate

The catchment lies in sub-humid tropical climatic zone. The mean annual temperature of the catchment is about 29°C. The maximum temperature of the region varies from 38.9°C to 44.4°C and the minimum temperature varies from 10.6°C to 20.6°C. Evaporation is ranging from 13.9 mm to 23.6 mm with the average of 20.9 mm/day during May-June (SCD, 1983). Precipitation occurs in the form of rainfall during July to September. July and August are the wettest months. The annual precipitation of the area is 1243 mm.

3.3 Topography

The catchment has extremely undulating and irregular slopes ranging from moderate 1.8% to steep 31.94%. The average slope of the catchment is 7.3%. The maximum elevation of the catchment is 675 m, the minimum elevation is 382 m above mean sea level (Fig. 3).

Fig. 2 Location map of Karso catchment

3.4 Soil Characteristics and Drainage Pattern.

The soil within the area is primarily coarse granular. The texture of soil is light sandy loam with the average percentage of coarse sand, fine sand, silt and clay as 30%, 28%, 17% and 25% respectively (Singhal, 1982). The data collected from soils Division of DVC Hazaribagh (Table 1), illustrates the characteristics of the soils of the catchments.

Table 1 Soil characteristics at Different Locations in the Karso Catchment

Location	Coarse Sand (%)	Fine Sand (%)	Silt (%)	Clay (%)	App. Density	% water Holding Capacity	Pore Space	Specific Gravity
Higher Elevation	55.30	29.20	7.03	7.73	1.37	27.00	36.57	2.08
Middle Elevation	35.40	26.68	14.75	21.83	1.38	29.67	40.22	2.06
Lower Elevation	14.55	33.28	21.20	29.65	1.40	33.52	43.96	2.09

The soils are low in organic matter content. The drainage pattern of the catchment is shown in Fig. 3. The main stream namely Kolhuwatari has several sub-tributaries spread over the entire area.

3.5 Land Use Pattern

The land use in this area can be grouped under three categories viz. agricultural land, forest and open scrub. The forests in the catchment are mainly of two types viz. protected forest and open forest. The protected forest is managed by forest department of Hazaribagh. The open forest has been defined as the area with less than 50% crown density and the dense forest has been defined having more than 75% crown density (Singhal, 1992). Agricultural land has paddy cultivation and mixed cultivation areas. Land use pattern in the catchment is shown in Fig. 4. Most of the cultivated area has been treated by soil conservation measures like terracing, bunding etc.

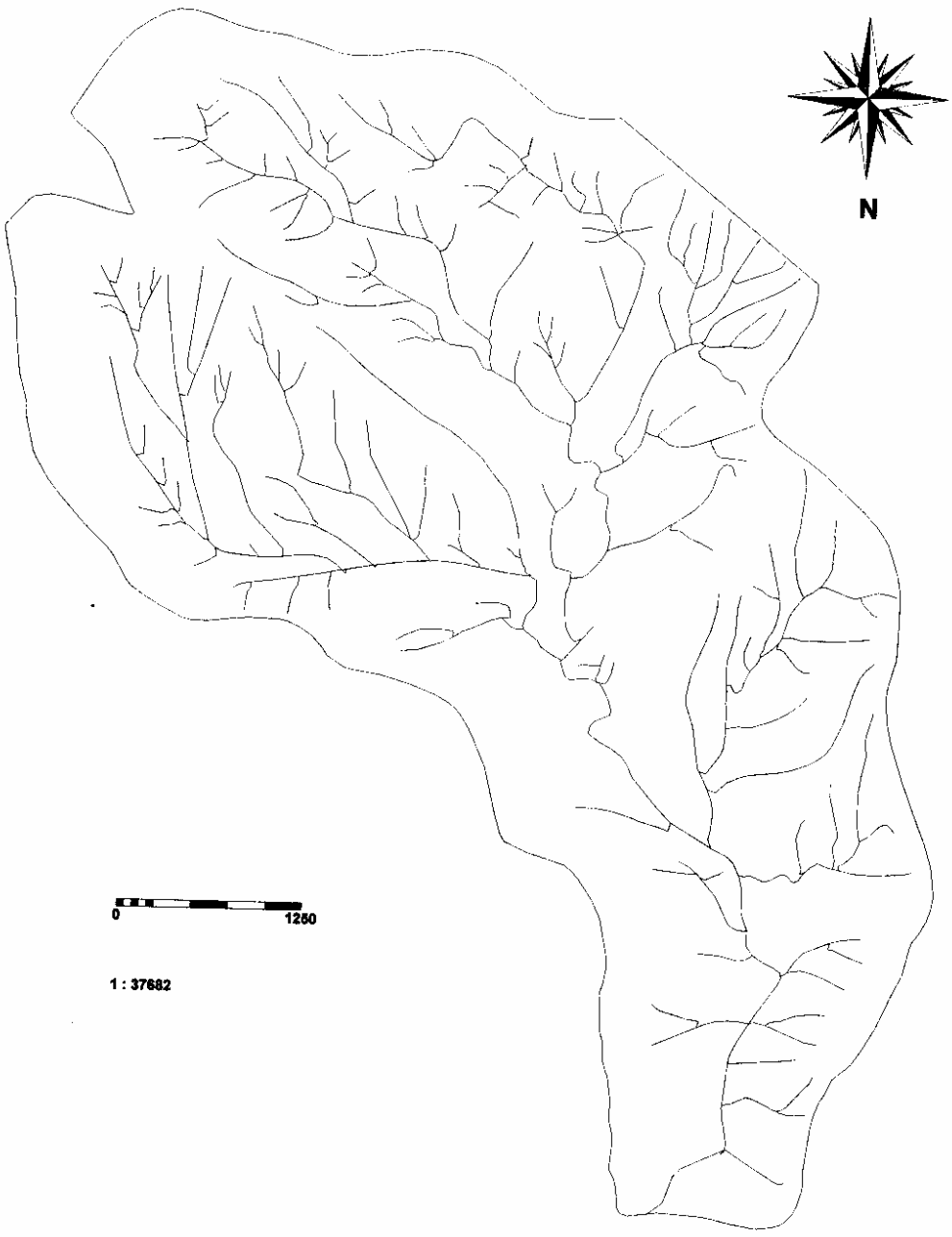

Fig. 3 Drainage map of Karso catchment

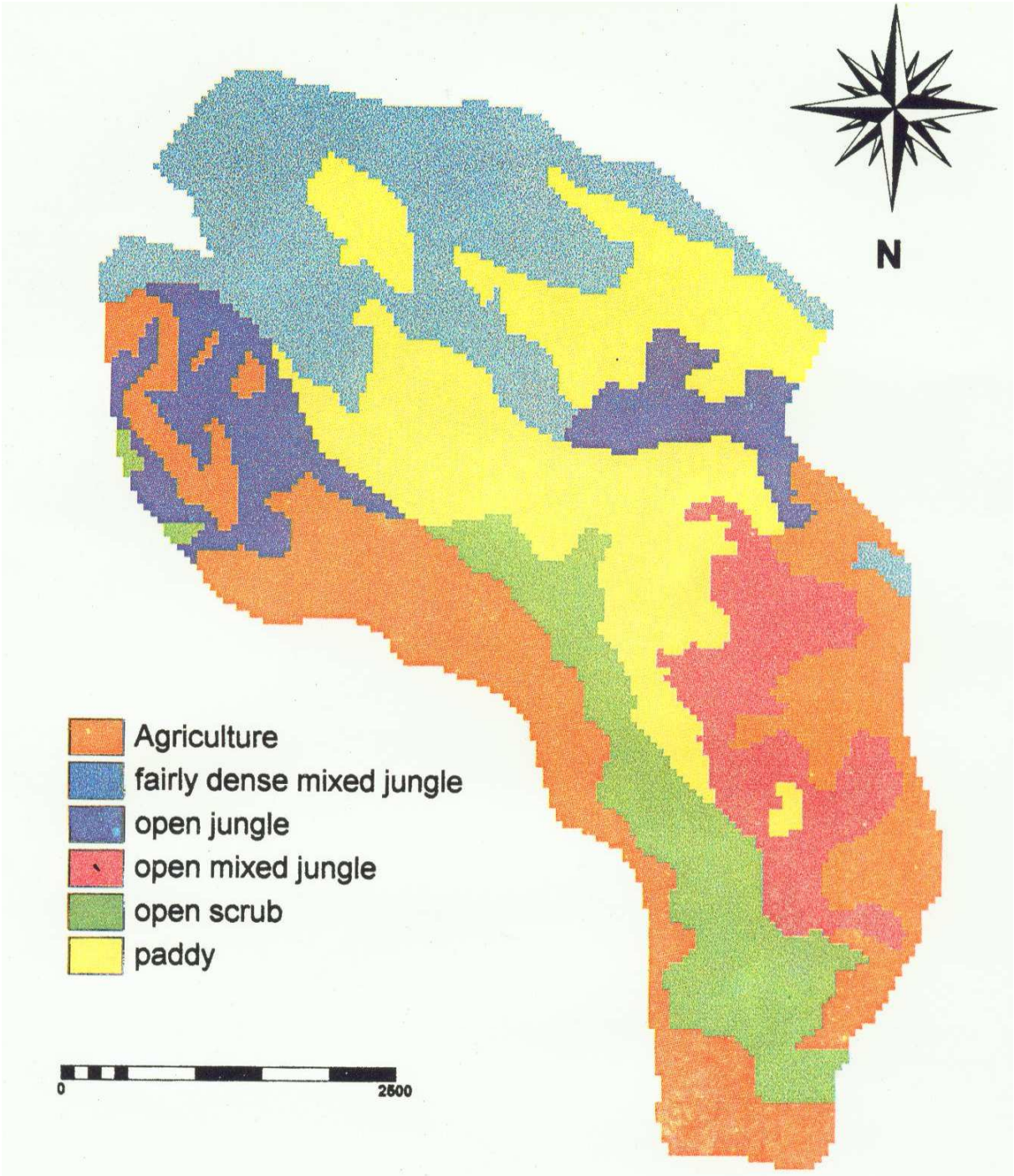

Fig. 4 Landuse map of Karso Catchment

3.6 Instrumentation, Measurement and Collection of Data.

The gauging work of Kohuwatari river flow and collection of sediment load data were initiated in the year 1991 for hydrological studies to assess the effects of soil conservation measures on surface runoff and erosion under the Indo-German Bilateral Project on Watershed Management (S&WCD, 1991). Under this scheme, existing and newly constructed sediment monitoring stations were equipped with tipping bucket type automatic rainfall recorder and water level recording devices, linked to an electronic data logger system. Samples for sediment load were collected using the Punjab or USDA bottles. Sediment samples were taken for every 15-cm of rise and fall of water level with a maximum time interval of one hour during a flood event. The data on rainfall, runoff and sediment yield for the catchment is available in the literature (S&WCD, 1991).

4. ANALYSIS

4.1 Generation of Digital Input Maps

The river network and contour map of the study area has been derived from Survey of India toposheets no 72H/7/SE and 72H/8/NE in 1:25,000 scale. Derived contour and drainage maps were then digitized on Integrated Land and Water Information System (ILWIS). Digitized segment contour map, rasterized to 30m-pixel size is then interpolated to generate a Digital Elevation Model (DEM) of the area. This DEM was further analysed to remove pits and flat areas in it using neighborhood functions available in ILWIS. Further a slope map and flow direction map is generated from this DEM. Figs. 5 and 6 show respectively the classified DEM of the basin and classified slope map of the basin.

4.2 Time Area Diagram

Velocity is a vector quantity specified by magnitude and direction of flow. In grid based GIS analysis, the direction of flow from one cell to other neighboring cell can be ascertained using pour point algorithm (ESRI, 1992). Once the pour point identified the flow direction in each cell, a cell to cell flow path exists to the watershed outlet. If a flow path from cell j to the outlet traverses m cells, $m = 1,2,.....M_j$, the flow length L_j is defined as the flow distances through each cell along the path

$$L_j = \sum_{m=1}^{M_j} l_m \qquad \ldots 33$$

where cell flow distance l_m is equal to the cell size or 1.41 times the cell size depending on whether the flow direction is along the coordinate axis or along a diagonal, respectively. If the flow time in cell m is T_m, the flow time T_j from cell j to the outlet can similarly be computed by summing the time through each of M_j cells on the path as

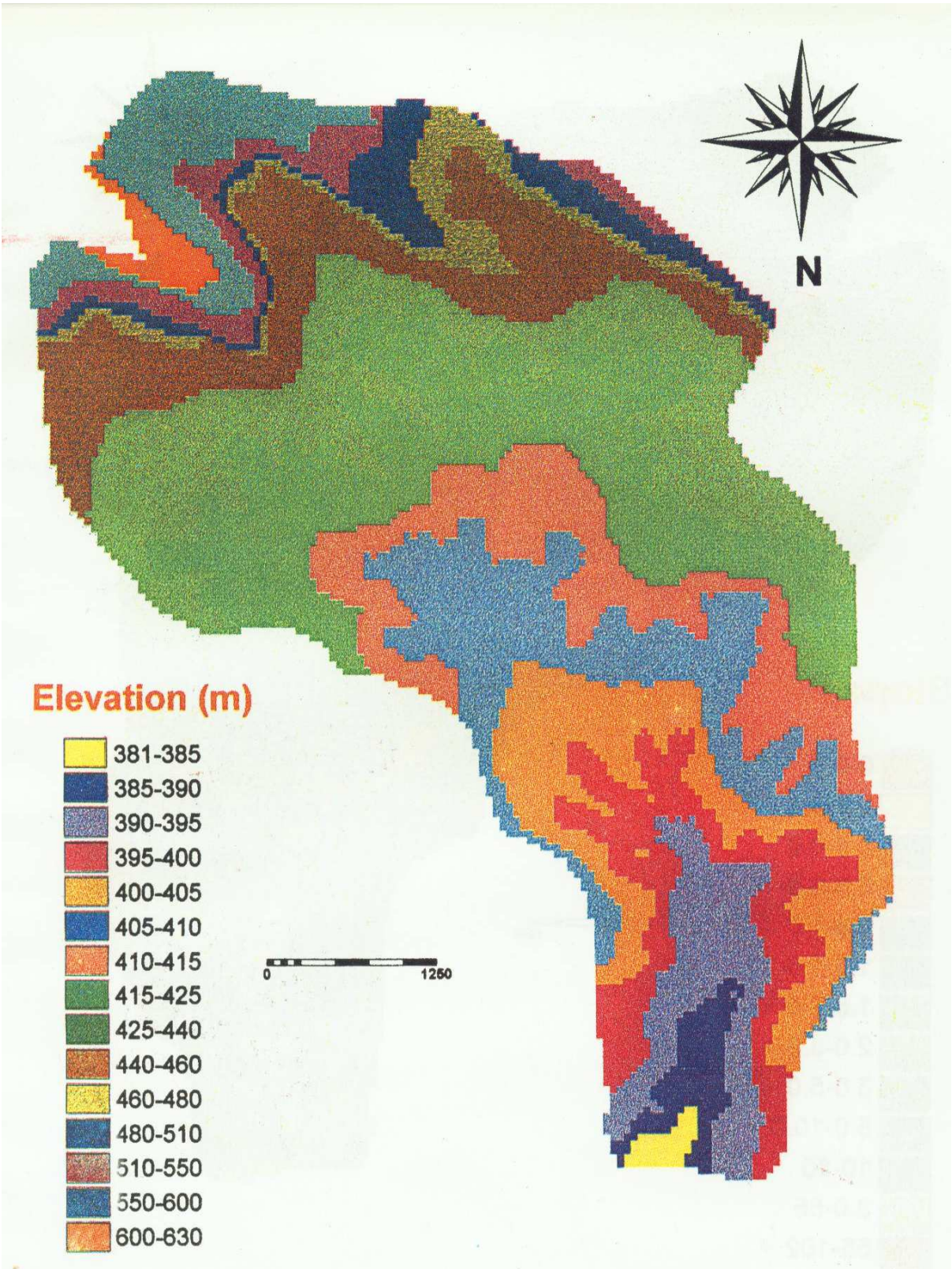

Fig. 5 Classified DEM of Karso Catchment

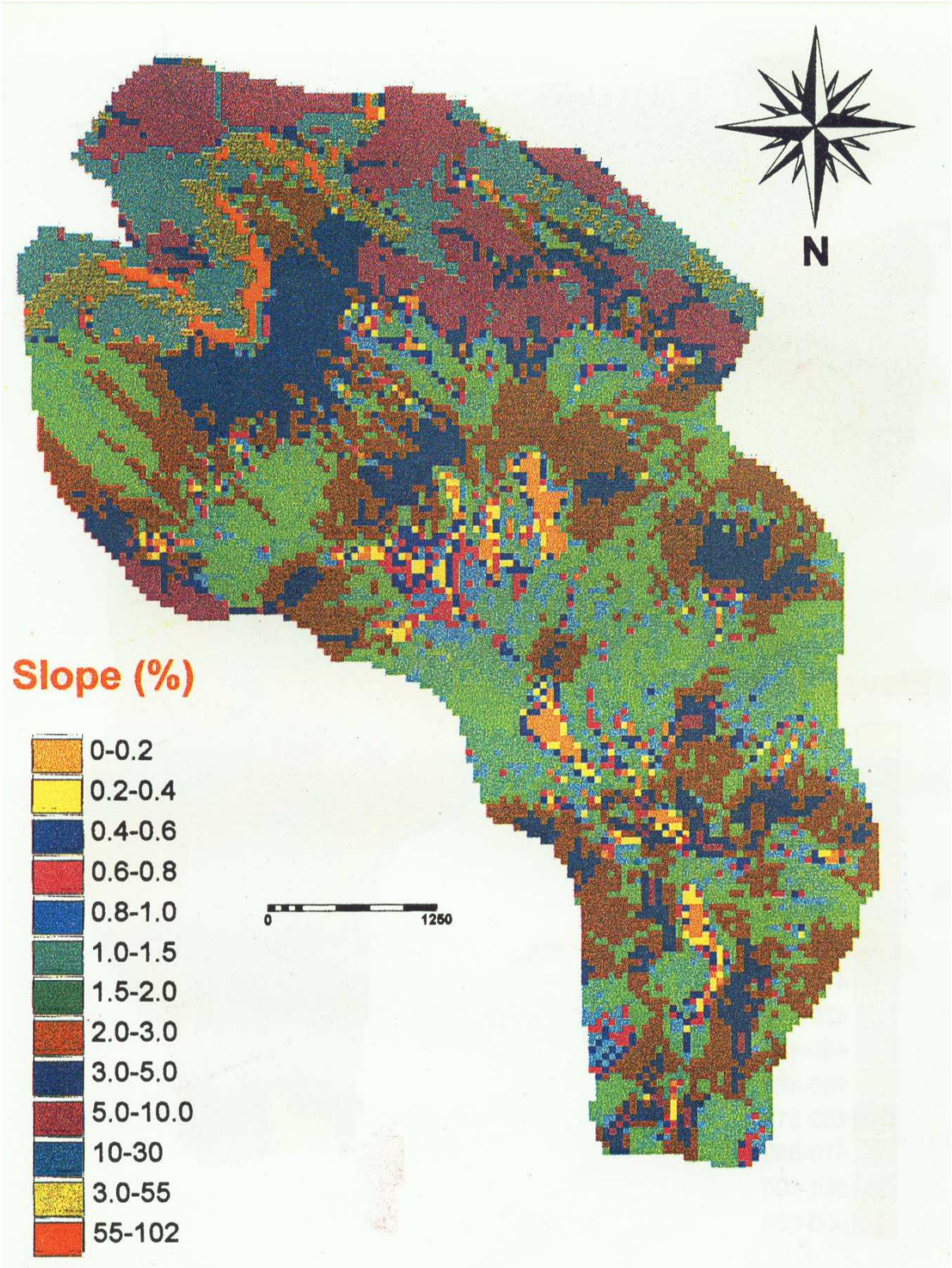

Fig. 6 Slope map of Karso catchment

$$T_j = \sum_{m=1}^{M} T_m \qquad \text{... 34}$$

Determination of flow time by the method described above requires the specification of the flow time for each cell on the watershed. There are a number of methods by which this can be done. However for the present study, method proposed by Regan and Duru (1972) for estimating travel time T_m over a plane surface based on kinematic wave equation have been employed. The equation is:

$$T_m = \frac{6.918(n \cdot L)^{0.6}}{i_e^{0.4} S_m^{0.3}} \qquad \text{... 35}$$

where T_m is travel time in minutes, n is Manning's n, L is length of cell in direction of flow in metre, i_e is rainfall intensity in mm/hr, S_m is slope of cell m. Since for each cell both flow direction and flow time area now known, and the paths from each cell to the watershed outlet has been specified, it follows that one can create a grid of flow travel times where the value in each cell is the time taken for water from that cell to flow to the watershed outlet. The cells may then be classified into zones i, $i=1,2,....$, whose travel time t falls into time interval $0 \leq t < \Delta t$, zone 2 has travel time $\Delta t \leq t < 2\Delta t$, and so on. The line bounding the outer limit of the cells in zone i is the isochrone of travel time $t=i\Delta t$ to the watershed outlet. The total area of the cells in zone i is A_i. In this way, the isochrone map of the watershed is created and is shown in Fig. 7.

4.3 Generation of Attribute Information

The time area diagram is further analysed to calculate area, length, width, average slope of each isochrone. The average slope of each isochrone was calculated by map cross between slope map and isochrone map and aggregate functions of ILWIS. Further Manning's n, USLE K and USLE C maps were prepared as attribute map of landuse map. For each isochrone, average value of Manning's n, USLE K and USLE C parameters

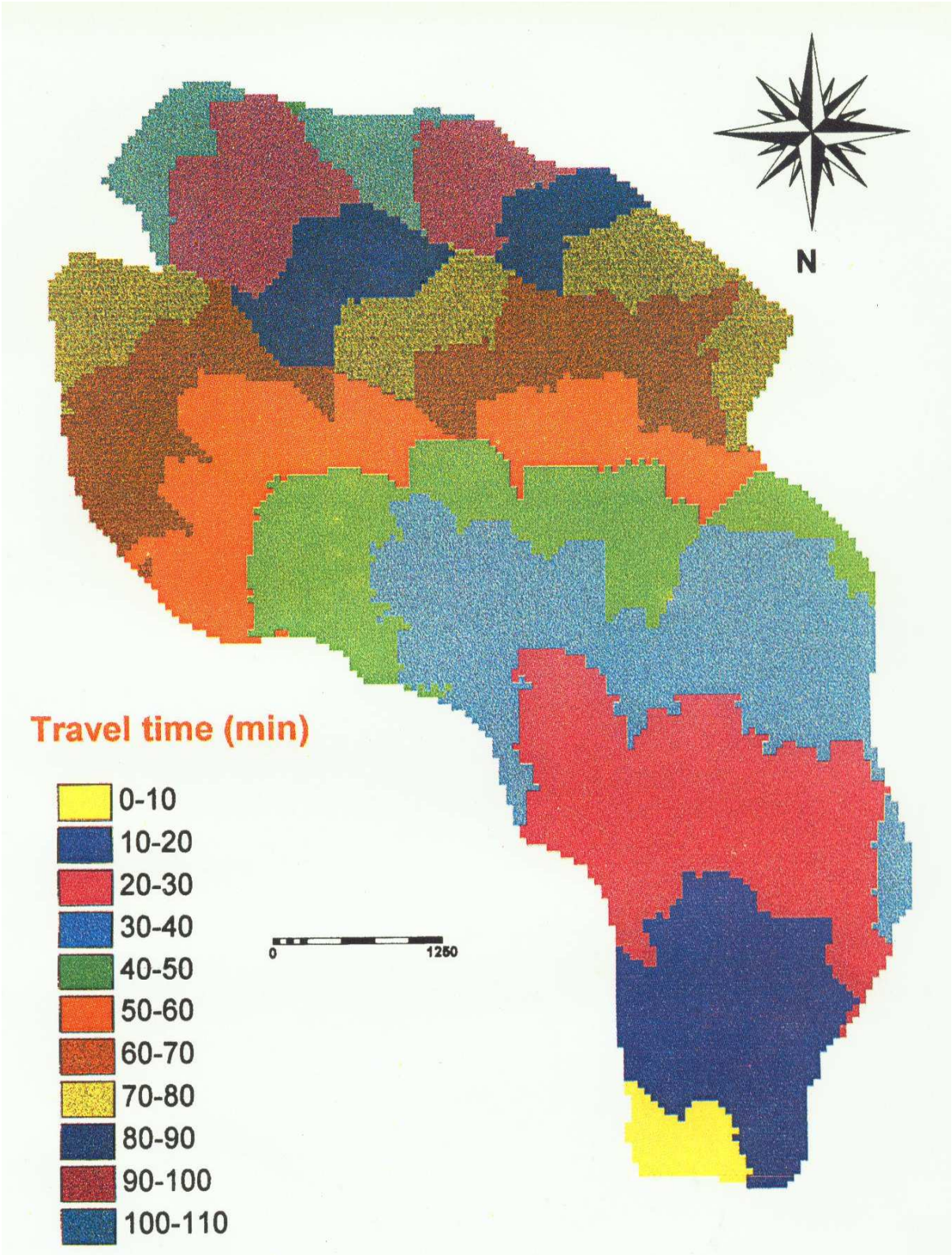

Fig. 7 Travel time map of Karso catchment

were calculated by cross operation between appropriate maps and further aggregation of resultant cross table into time area zones. Results of these cross and aggregation operations are shown in Table 2.

Table 2 Characteristics of time-area segments of Karso catchment

Segment	Area sq. m	Width M	Length m	Mann. n	Slope m/m	USLE C	USLE K
0-10	440000	700	628.57	0.20000	0.02340	0.20	0.28
10-20	2562500	1700	1507.35	0.10405	0.01910	0.27	0.58
20-30	3885000	2550	1523.53	0.14627	0.01810	0.26	0.42
30-40	4642500	3400	1365.44	0.19817	0.01610	0.25	0.39
40-50	3115000	4000	778.75	0.31096	0.02070	0.24	0.44
50-60	3080000	4200	733.33	0.32934	0.02600	0.25	0.36
60-70	3100000	3600	861.11	0.35690	0.06350	0.22	0.36
70-80	2567500	3500	733.57	0.41908	0.13740	0.16	0.36
80-90	1535000	2350	653.19	0.46837	0.13510	0.10	0.33
90-110	1955000	2200	888.64	0.48913	0.17360	0.05	0.24
110-120	1052500	1600	657.81	0.50000	0.11900	0.02	0.20

5. RESULTS AND DISCUSSIONS

For the purpose of numerical computations the computational time period Δt, was considered to be equal to the discretization time T as adopted for preparation of time area segments. Since for the Karso catchment, the observed rainfall-runoff sediment yield data were available at 10-minutes interval, the discretization time T was considered equal to 10 minutes. The length of time-area segment determined the spatial grid size Δx. As the length is different for different time-area segments (Table 2) in a catchment, non-uniform spatial grid as determined by these lengths was formed.

5.1 Calibration of rainfall-runoff model

The value of Manning's friction parameter n lying between 0.01 and 0.5 were chosen as per Woolhiser (1977) based on the landuse of the catchment. The time-area map was superimposed over Manning's n value map and aggregated value of Manning's n for each time-area segment was calculated. The kinematic friction parameter α was then computed using eq. 6 by taking ξ as 1.0. The value of other parameter β in the kinematic formulation was kept constant and equal to 0.6.

Rainfall abstraction was carried out using phi index method. The phi index depends upon antecedent moisture conditions and it was determined for each event by a volume matching in which the rainfall excess volume was equal to direct runoff volume. Using non-dimensional effective rainfall, roughness coefficient, and kinematic parameters as computed previously, the initial estimates of Q_{i+1}^{j+1} were computed with $\beta=1$ for two storm events selected for calibration. Next the estimates for Q_{i+1}^{j+1} was obtained using eq. 21, using the initial estimates obtained with linear scheme above for both the events. These values were later dimensionalized by making use of appropriate definitions. The outputs obtained include discharge and velocity at each computational grid point and outflow hydrograph at the outlet. The value of model parameter ξ was optimized using

Marquart algorithm. After successful execution of the optimization model the parameter ξ was found to be 0.14674 as optimum for Karso catchment. Comparison statistics of observed and simulated events is given in Table 3 for model calibration run. Nash-Sutcliffe (1970) coefficient R^2 was also calculated for both the events used in model calibration. As can be seen from Table. 3 the model efficiency is found to be above 0.88 for model calibration. Graphical comparison of observed and simulated hydrographs for both the events used in calibration are shown in Figs. 8 and 9 respectively. It can be seen from these plots, that the model can very well simulate runoff hydrograph used in calibration.

Table 3 Comparison of observed and simulated runoff for calibration

Event	Peak flow (cumec)		Time to peak flow (min)		Volume (mm)		Nash-Sutcliffe R^2
	Obs.	Sim.	Obs.	Sim.	Obs.	Simu.	
03.08.91	4.130	3.539	500	520	4.71	4.67	0.8875
04.08.91	3.855	3.667	280	280	4.97	4.92	0.8993

5.2 Verification of rainfall-runoff model

The calibrated model was used for verification of independent set of three storm events whose data was not used for calibration. Optimized value of model parameter ξ found out during model calibration was used to compute flow velocities and discharge at all the computational grid points as well as catchment outlet. The verification results are presented in Table 4. To ascertain applicability of the model, Nash-Sutcliff coefficient R^2 was also calculated and is given in Table 4. For storm events used in validation the R^2 values were found to range between 0.7 to 0.9. Comparison between computed and observed values of peak discharge and time to peak discharge is also shown in Table 5. Graphical comparison of observed and simulated hydrographs is shown in Figs. 10-12. These results verify suitability of present method for simulation of rainfall runoff storm events.

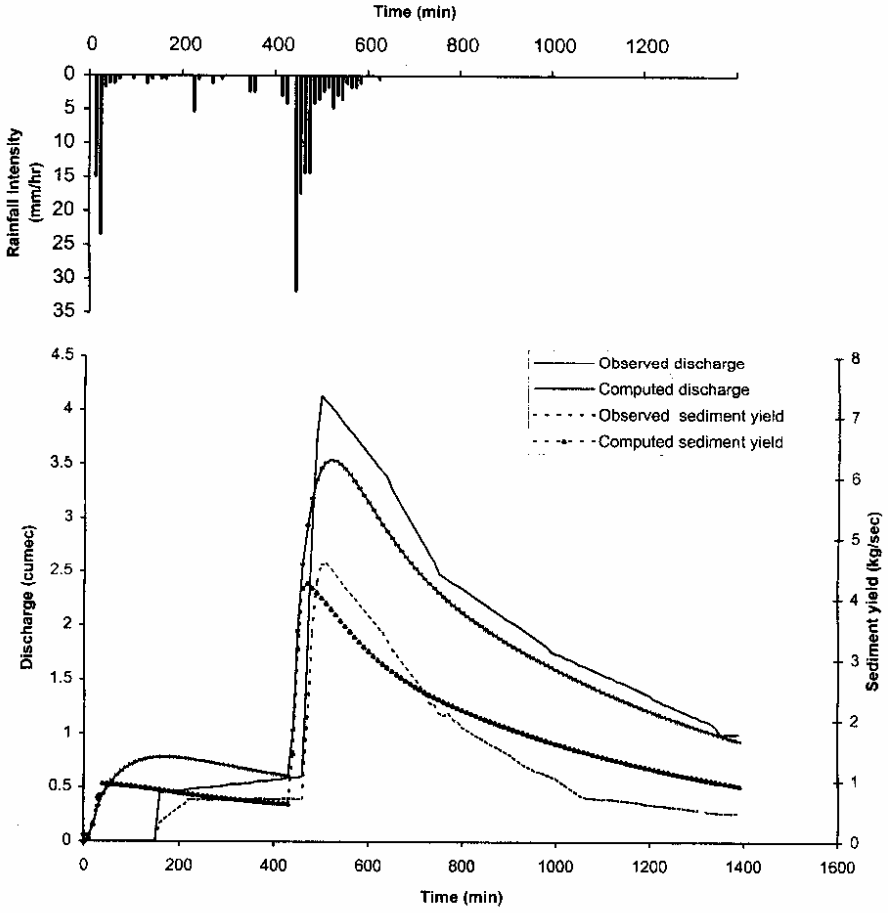

Fig. 8 Comparison of observed and simulated discharge and sediment yield (03.08.1991)

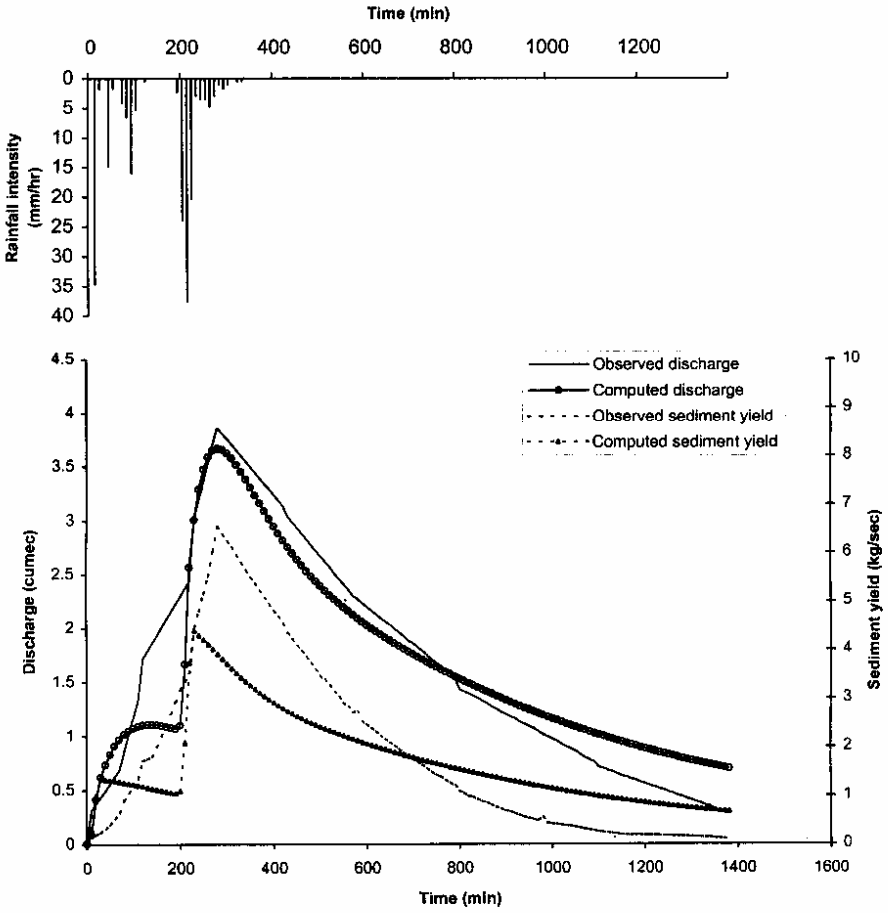

Fig. 9 Comparison of observed and simulated discharge and sediment yield (04.08.1991)

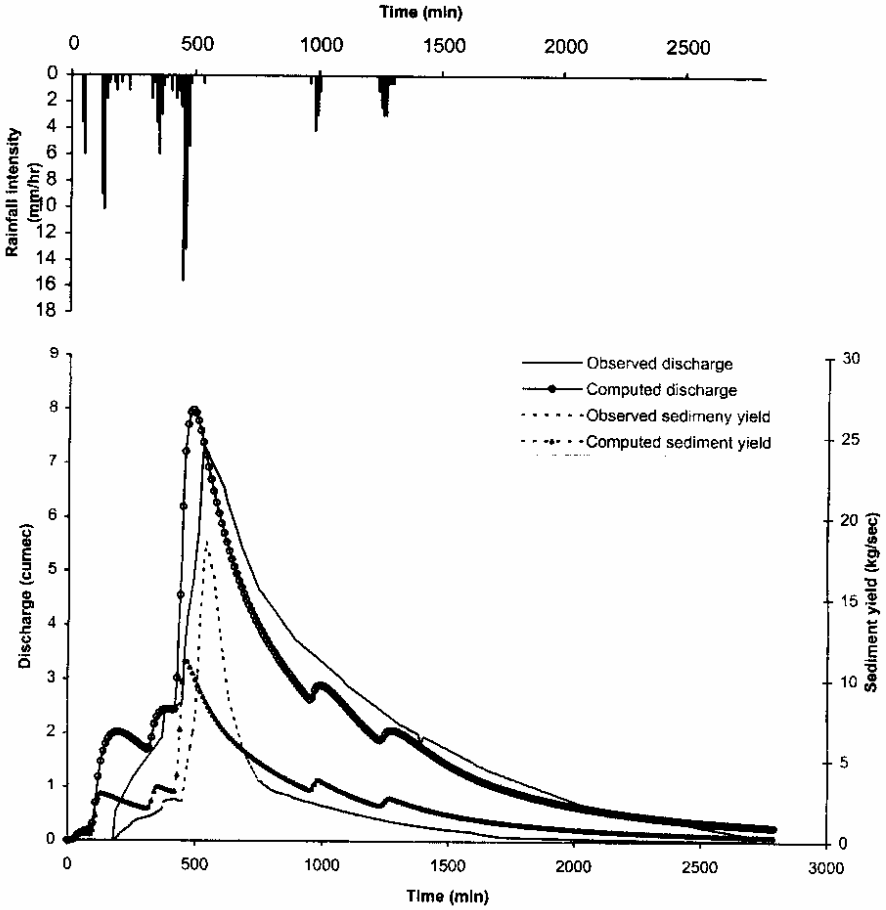

Fig. 10 Comparison of observed and simulated discharge and sediment yield (17.08.1991)

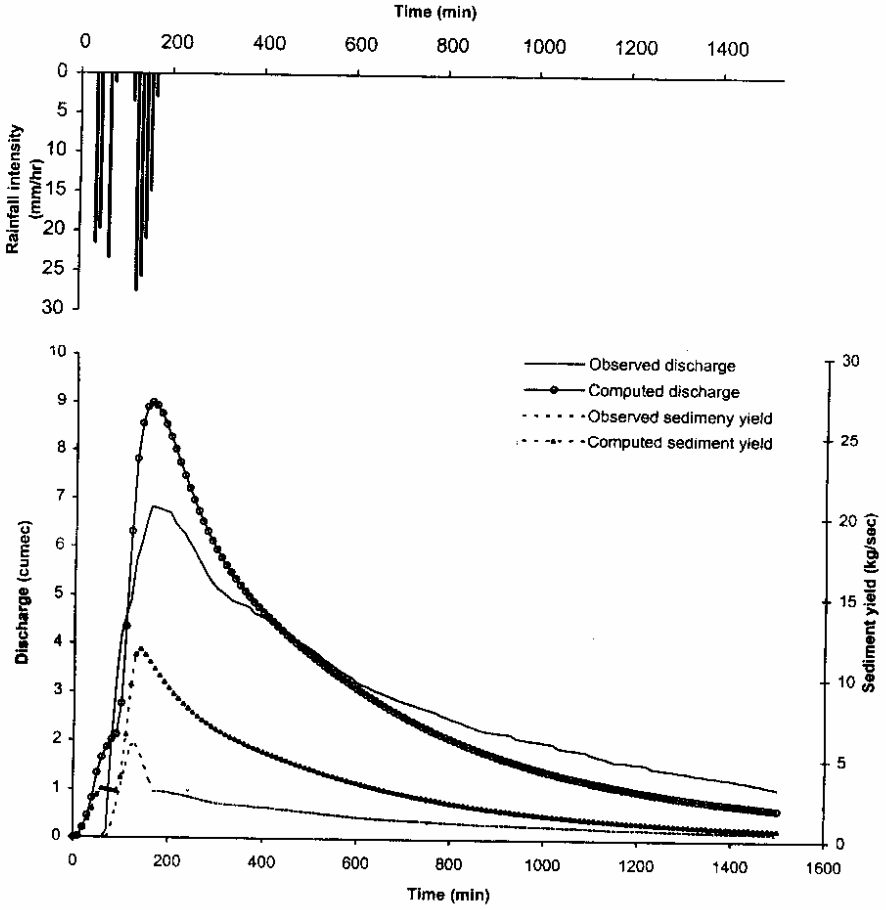

Fig. 11 Comparison of observed and simulated discharge and sediment yield (27.07.1991)

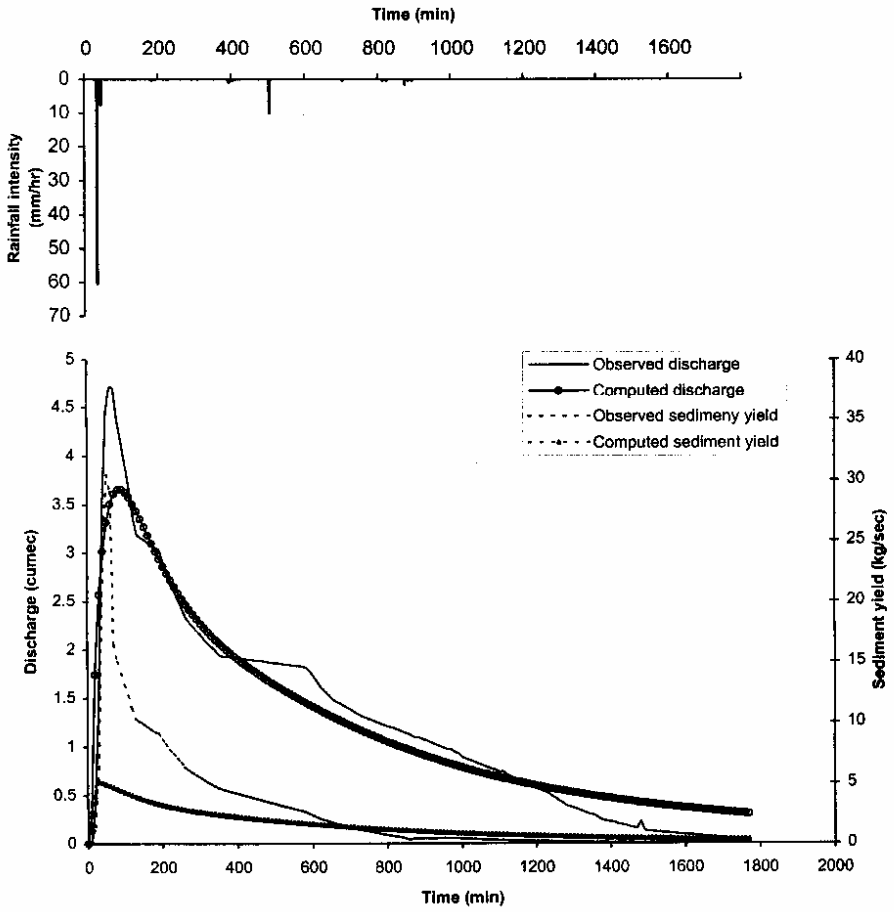

Fig. 12 Comparison of observed and simulated discharge and sediment yield (28.07.1991)

Table 4 Comparison of observed and simulated runoff for validation

Event	Peak flow (cumec)		Time to peak flow (min)		Volume (mm)		Nash-Sutcliffe R^2
	Obs.	Sim.	Obs.	Sim.	Obs.	Simu.	
17.08.91	7.250	7.991	540	490	11.30	11.21	0.8375
27.07.91	6.830	9.000	160	160	9.23	9.13	0.8082
28.07.91	4.717	3.656	60	90	4.75	4.63	0.9297

5.3 Sediment yield estimation

Sediment yield estimations were made using known flow velocity and discharge computed by flow model at each computational grid points using numerical solution of sediment continuity equation given by eq. 26. Attribute information such as USLE K and C, slope of each time-area segment etc. for all discritized time area segments was derived using GIS analysis and reported in Table. 2 have been used for computation of sediment yield. The mathematical formulation for sediment yield estimation has four parameters viz. C_{f1}, C_{f2}, C_{a1} and C_{a2}. The parameters C_{f1}, and C_{f2} were taken as 161 and 16,320 respectively as per Beasley et al. (1991). The parameters C_{a1} and C_{a2} were optimized using sediment yield data for two storm events used for rainfall-runoff model calibration so as to obtain minimum standard error between observed and computed sediment yield. Accordingly, value for C_{a1} and C_{a2} was found to be 0.002 and 0.000065 respectively for Karso catchment.

Comparison was made between observed temporal variation of sediment yield and corresponding computed values for both the events used for calibration. Table 5 gives comparison for the peak value of sediment yield, time to peak value of sediment yield as well as Nash-Sutcliffe R^2 value for both the events. Graphical comparison of computed and observed temporal variation of sediment yield for events used in calibartion is shown in Figs. 8 and 9. It is evident from these plots that in general, satisfactory prediction is obtained for temporal variation in sediment yield.

Table 5 Comparison of observed and simulated sediment yield for calibration

Event	Peak Sediment discharge (kg/min)		Time to peak sediment discharge (min)		Total sediment yield (Tons)		Nash-Sutcliffe R^2
	Obs.	Sim.	Obs.	Sim.	Obs.	Simu.	
03.08.91	274	255	510	470	109.00	137.67	0.7094
04.08.91	393	263	280	230	156.25	142.39	0.6843

To check the applicability of optimized values of parameters C_{a1} and C_{a2}, data for remaining three events have been used for model verification. The same data have also been used for verification of rainfall-runoff model. The comparison between corresponding observed and computed values for verification data is given in Table. 6. It can be seen from Table 6 that the model simulated independent data set reasonably well. Poor prediction in case of one storm event may be attributed to uncertainity in observed data. Graphical comparison of computed and observed temporal variation of sediment yield for events used for model verification has been shown in Figs. 10-12. It is evident from these plots that in general, satisfactory prediction is obtained for temporal variation in sediment yield.

Table 6 Comparison of observed and simulated sediment yield for validation

Event	Peak Sediment discharge (kg/min)		Time to peak sediment discharge (min)		Total sediment yield (Tons)		Nash-Sutcliffe R^2
	Obs.	Sim.	Obs.	Sim.	Obs.	Simu.	
17.08.91	1104	667	540	460	287.53	385.97	0.6248
27.07.91	341	698	130	140	117.67	293.49	--
28.07.91	1826	310	50	30	283.49	156.98	0.3160

Total sediment yield was also computed for all the events and is given in Table 5 and 6 both for calibration and verification. Comparison of total sediment yield reveal that the present method has predicted total sediment yield with reasonable accuracy for majority of events.

6. Conclusions

GIS techniques have been utilized to spatial discretization of a catchment in to time-area segments to be used in numerical solutions of the governing differential equations for rainfall-runoff-erosion process. Various thematic layers such as soil, landuse, slope, flow direction, DEM were generated for the Karso catchment using various tools available in GIS. These thematic layers were further utilized to generate attribute information such as Manning's n, USLE K and C parameters for use in rainfall-runoff-soil erosion model. Based on DEM and related attributed information of the catchment, time-area map of the catchment was prepared and used for spatial discretization of the catchment. Comparison of results indicate applicability of this modelling concept for Karso catchment.

REFERENCE

Abott, M.B., Bathrust, J.C., Cunge, J.A., O'Connel, P.E. and Rammussen, J. 1986. An introduction to the European Hydrologic System - Systeme Hydrologiuqe European, SHE. J. of Hydrology, 87: 45-59.

Ashida, K . Takahashi, T., Sawada T., 1976. Sediment yield and transport on a mountainous small watershed, Bulletin of the Disaster Prevention Research Institute, Kyoto University, Vol. 26, Part 3, No. 240: 119:125:125. Kyoto , Japan

Beasley, D.B., Huggins, L.F., and Monk, J.E. 1980. ANSWERS: A model for watershed planning, Trans. Am. Soc. Agric. Eng., 23, 938-944.

Beasley, D.B., and Huggins, L.F. 1991. ANSWERS: Users mannual. Publication Number 5, Agricultural Engineering Department, UGA-CPES, University of Georgia, USA.

Bennett, J.P., 1974. Concepts of mathematical modelling of sediment yield, Water Resources Res. 10, 3, 485-492.

Chow, V. T., Maidment, D.R., Mays, L.W., 1988. Applied Hydrology. McGraw Hills Book Company, Singapore, pp. 272-309.

Field, W.G., 1982. Kinematic wave theory of catchment response with storage, J. Hydrol., 55 (1-4), 279-301.

Field, W.G. and Williams, B.J. 1983. A generalised one dimensional kinematic catchment model. J. Hydrol., 60: 25-42.

Foster, G.R., 1982. Modelling the erosion process. In: C.T. Hann, H.P. Johnson and D.L. Brakensiek (Editor), Hydrologic Modelling of Small Watersheds, ASCE Monograph No. 5, Proc. ASCE, St. Joseph, Michigan , pp. 297-382.

Henderson, F.M., 1966. Open Channel Flow, Chs. 8 and 9, Collins Macmillan, London, pp. 285-404.

Knisel, W.G. (Editor), 1980. CREAMS: A field scale model for chemicals, runoff and erosion for agricultural management systems, US Department of Agricultural Conservation Research Report No. 26.

Kothyari, U.C., Tiwari, A.K. and Singh, R. 1994. Prediction of sediment yield. Jr of Irrigation and Drainage Engg., Proc. ASCE, 120(6): 1123-1131.

Kothyari, U.C., Tiwari, A.K. and Singh, R. 1996. Temporal variation of sediment yield. Jr. of Hydrol. Engg., Procd. ASCE, 1(4): 169-176.

Laguna, A., Giraldez, J.V., 1993. The description of soil erosion through a kinematic wave model, J. Hydrol., 145, 65-82.

Laurenson, E.M. 1964. A catchment storage model for runoff routing, J. Hydrol. 2, 141-163.

Linsley, R K. Kohler, M.A., Paulhus, J.L., 1958. Hydrology for Engineers, McGraw Hills Book Company Inc., New York, pp. 237-239.

Maidment, D.R., 1993. Developing a spatially distributed unit hydrograph by using GIS, IAHS Publ. No.211, 181-193.

Meyer, L.D., and Wischmeier, W.H. 1969. Mathematical simulation of the process of soil erosion by water. Trans. Am. Soc. Agric. Eng. 24(6):1472-1475.

Nearing, M.A., Foster, G.R., Lane, L.J. and Finkener, S.C. 1989. A process based soil erosion model for USDA water erosion prediction project technology, Trans. ASAE, 32 (5), 1587-1593.

Regan, R.M. and Duru, J.O. 1972. Kinematic wave nomograph for time of concentration. Proc. Am. Soc. Civil Eng. 98(HY10): 1765-1771.

Singh, V.P., 1989. A quasi-conceptual linear model for synthesis of direct runoff with potential application to ungauged basin. Military Hydrology Report No. 17, Dept. of Civil Engg. Louisiana State University, Baton Rouge, LA, USA, pp. 30

Tiwari, A.K., 1995. Temporal variation of sediment yield from small catchments, Ph.D. Thesis, Dept. of Hydrology, University of Roorkee, Roorkee, India, 267 pp.

Vanliew, M.W., Saxton, K.E., 1984. Dynamic simulation f sediment discharge from agricultural watersheds, Transactions of the ASAE, 27 (4), 1087-1092.

Walling, D.E., 1988. Erosion and sediment yield research - some recent perspectives, J. Hydrol. 100, 113-141.

Wicks, J.M. Bathurst, J.C.,1996. SHESED: A physically based, distributed erosion and sediment yield component for the SHE hydrological modelling system, J. Hydrol., 175, 213-238.

Williams, J.R. 1978. A sediment graph model based on instantaneous unit sediment graph. Water Resources Research, 14(4): 659-664.

Wischmeier, W.H. and Smith, D.D. 1978. Predicting rainfall erosion losses. Agriculture Handbook No. 537, USDA - Science and Education Administration: 58.

Woolhiser, D.A., 1977. Unsteady free surface problems in mathematical models for surface water hydrology. In: T.A. Marions, and J.R. Wallis (Editors), A Wiley Interscience Publication, Chickester, pp. 195-213.

Wu, T.H., Hall, J.A. and Bonta, J.V. 1993. Evaluation of runoff and erosion models. Jr. of Irrigation and Drainage Engg., Procd. ASCE, 119(4):364-382.

Young, R.A., Onstad, C.A., Bosch, D.D. and Anderson, W.P. 1987. AGNPS: An agricultural non point source pollution model. Conservation Research Report 35, U.S. Deptt. of Agric. Res. Services, Washington, D.C.

DIRECTOR: *S.M. Seth*

DIVISIONAL HEAD: *B. Soni*

STUDY CONDUCTED BY: *M.K. Jain*
Scientist C